Basic transverse dynamics of a photorefractive oscillator

Daniel Hennequin, Laurent Dambly, Didier Dangoisse, and Pierre Glorieux

Laboratoire de Spectroscopie Hertzienne, Unité Associée au Centre National de la Recherche Scientifique, Université des Sciences et Technologies de Lille, F-59655 Villeneuve d'Ascq Cedex, France

Received April 29, 1993; revised manuscript received September 28, 1993

The basic phenomena of transverse dynamics of a two-wave mixing photorefractive oscillator (PRO) in the weakly multimode case are considered. The evolution of the transverse patterns as a function of two control parameters, namely, the cavity length and the PRO gain, is investigated. The behavior is described in terms of the modes of the empty cavity. It is found that the mode interactions occur differently, depending on whether the modes belong to the same frequency-degenerate family or not, although in both cases the observed behavior is periodic.

1. INTRODUCTION

In the study of the spatiotemporal dynamics of nonlinear optical systems and the search for optical turbulence there has been an increase of interest in the transverse patterns observed in these systems.[1–14] Most experimental and theoretical studies are devoted to lasers and pursue one of two research lines. The first concentrates on the dynamics of systems with small numbers of modes and uses a decomposition of the electric field on the modes of the empty cavity.[1–4] The second follows a global approach similar to that used in hydrodynamics[5–7]; in particular, equations of the laser near threshold have been demonstrated to be equivalent to the complex Ginzburg–Landau equation.[8] In optical cavities the Fresnel number $\mathcal{N}_F$ characterizes the system size, just as the aspect ratio does in hydrodynamics. When $\mathcal{N}_F$ is small, the description in the empty-cavity mode bases is still relevant, because the number of modes remains small, while in systems with large $\mathcal{N}_F$ it is more suitable for one to adopt a global viewpoint in which optical turbulence or defects can be described. As far as transverse patterns are concerned, it is remarkable that lasers have been considered experimentally mostly in the low $\mathcal{N}_F$ limit, while the large $\mathcal{N}_F$ case has been approached only in other systems, such as photorefractive oscillators (PRO's), hybrid optical valves, or resonators containing nematic liquid crystals.[9–11] The low-$\mathcal{N}_F$-limit investigation of lasers has shown that the few-mode case could also lead to rich spatiotemporal dynamics.[1–3] Moreover, this case retains the possibility of a detailed comparison between experimental and theoretical results.[1] For example, the observation of stationary and, more recently, of periodically moving phase singularities in lasers, demonstrated by Brambilla *et al.*,[1,2] provides a clear example of the efficiency of this approach.

In that regard it is interesting to consider the basic phenomena of transverse dynamics in a PRO in the weakly multimode case, i.e., $\mathcal{N}_F$ of the order of several units.[12–15] Previous investigations of such weakly multimode PRO's have shown that a rich phenomenology can be expected, since even the monomode behavior has been found to be chaotic in a phase-conjugate PRO.[14,15] Moreover, periodic alternation and chaotic itinerancy have been observed in a two-wave mixing (2WM) PRO when the cavity symmetry is artificially broken.[13] However, these studies have concentrated on a local approach in the parameter space; i.e., they have been carried out for a fixed set of parameters. In contrast, we consider a global description; i.e., we have studied experimentally how the transverse patterns evolve as two control parameters, namely, the cavity length and the PRO gain, are changed in the weakly multimode 2WM PRO.

This paper is organized as follows. After a description of the experimental setup in Section 2, in Section 3 we analyze the response of the system as a function of the control parameters mentioned above and show that, in spite of a very narrow gain bandwidth (~10 Hz), the behavior is governed by the resonances of the empty-cavity modes grouped in families, as was demonstrated for lasers.[1] The details of the dynamics inside each family is examined in Section 4. It is shown that stable patterns of the PRO are either stationary as in lasers or periodic. The processes leading to dynamical regimes involving modes of the same family, and in particular their origin and frequencies, are discussed. Section 5 deals with the interaction between two families. The dynamics arising from the competition between modes from two different families is shown to differ from that occurring inside a single family, and the underlying processes leading to this difference are examined.

2. EXPERIMENTAL SETUP

A scheme of the experimental setup is shown in Fig. 1. The ring cavity is limited by two or three plane mirrors and one spherical mirror with a radius of curvature of 1 m. The cavity length is varied between 1 and 2 m and sets the value of the ratio $\Delta\nu_T/\Delta\nu_L$, where $\Delta\nu_L$ is the free spectral range and $\Delta\nu_T$ is the frequency spacing between transverse modes. The Fresnel number is limited by an iris inserted into the cavity and may be varied from 1 to ~100. The external coupling of the cavity, performed by means of a beam splitter, is 10%. A $Bi_{12}GeO_{20}$ (BGO)

0740-3224/94/040676-09$06.00

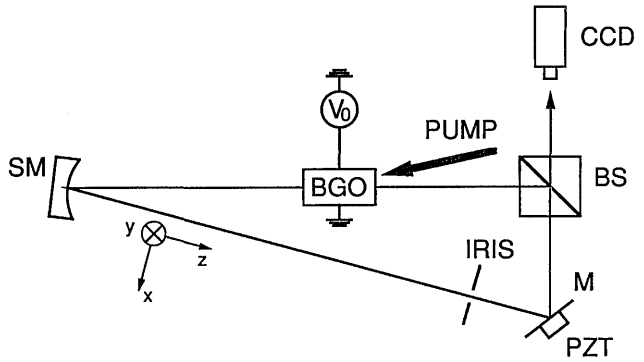

Fig. 1. Experimental setup of the 2WM PRO. The cavity is limited by spherical mirror SM, plane mirror M, and beam splitter BS used as a coupler. The piezoelectric translator, PZT, permits the cavity length to be varied.

photorefractive crystal is inserted into the cavity and is responsible for additional losses of 70%. The total losses are estimated to be 75% per round trip, so that the passive cavity linewidth $\Delta\nu_c$ is approximately $\Delta\nu_L/2.1$. The gain bandwidth $\Delta\nu$ of a 2WM PRO, centered on the frequency ν_0, is related to the detuning between the pump frequency ν_p and ν_0, and so is of a few hertz; this leads to a situation drastically different from that of the usual lasers. In particular, the frequency pulling, proportional in a first approximation to the ratio $\Delta\nu_c/\Delta\nu$, will be such that the emission frequency ν always remains close (at the scale of some hertz) to ν_0.[16] Another difference comes from the split, $\Delta\nu_a$, in degenerate frequencies that is induced by astigmatism. Although $\Delta\nu_a$ has not been measured in our experiments, it is clear that because of the use of an off-axis spherical mirror it has a value of several hundred kilohertz. In lasers the relative values $\Delta\nu_c \ll \Delta\nu_a \ll \Delta\nu$ result in well-separated frequency domains, while here, because $\Delta\nu \ll \Delta\nu_a \ll \Delta\nu_c$, the astigmatism induces a slight shift of wide resonances.

The crystal is pumped by a frequency-doubled Nd^{3+}:YAG laser at $\lambda = 532$ nm and with a typical intensity of 10 mW/cm^2. A dc voltage V_0, which is directly related to the gain of the 2WM, is applied to the crystal. Because the response time of the BGO crystal is ~0.1 s, we use a CCD camera as a detector; its 25-Hz frequency sampling is fast enough to analyze the dynamics of the system. However, a fast pointwise detector is used to confirm that no faster dynamics occurs.

Because of the long time scales involved in these experiments, special care has been taken with respect to the stability of the cavity length. For standard observations the cavity length is only passively stabilized, resulting in a residual drift of the order of 2 μm/h. However, in a test of whether stationarity can be reached in multimode operation, the cavity is actively stabilized by an interferometric method, improving the stability by a factor of 2. The residual drift is small enough to resolve any ambiguity between the intrinsic dynamics of the PRO at the time scale of the pattern evolution, which is typically 1 s, and the possible dynamics induced by variations in the length of the cavity, at the scale of 1 min or more.

The transverse patterns of the field can be projected onto the modes of the empty cavity. The Gauss–Hermite or the Gauss–Laguerre basis may be used. We introduce here the notation used below. An eigenmode of the Gauss–Hermite basis will be denoted H_{nm}, with n and m being the x- and the y-axis indices, respectively. An eigenmode of the Gauss–Laguerre basis will be denoted A_{pli}, with p and l being the radial and the angular indices, respectively, and $i = 1$ ($i = 2$) corresponding to the cosine (sine) mode. Modes associated with the same number $q = n + m = 2p + l$ have the same frequency in the empty cavity and so form a frequency-degenerate family, according to the terminology introduced in Ref. 1. Thus mode $H_{00} = A_{00}$ belongs to the $q = 0$ family, modes $H_{10} = A_{011}$ and $H_{01} = A_{012}$ to the $q = 1$ family, etc. The results presented below are related only to weakly multimode situations, i.e., cavities in which modes associated with a q larger than some critical value q_c are inhibited by the intracavity iris. In these experiments q_c takes values from 3 to 6, typically.

The symmetry of the cavity appears to play a key role in the behavior of the PRO. In particular, we notice that the PRO is able to oscillate even if the cavity is only roughly aligned, leading to drastically distorted patterns. Arecchi *et al.*[13] also mention that chaotic itinerancy was observed only in a tilted cavity. Therefore during our experiments we have carefully checked the alignment of the cavity. We have also tried to evaluate more precisely the role of the cavity symmetry in the dynamics of the system. For this purpose we use the fact that in a cavity with an odd number of mirrors the symmetry of the cavity is altered because of the inversion phase acquired by the modes that are antisymmetric with respect to the y axis (y-antisymmetric modes) after one round trip in the cavity, where the x and the y axis, respectively, are in and perpendicular to the plane of the cavity, as shown in Fig. 1.[17] As a consequence the dynamics observed in an odd cavity results only from the mode mixing, whereas the dynamics observed in an even cavity may also result from the lack of strongly preferred transverse axes.

As is mentioned above, the Fresnel number $\mathcal{N}_F$ plays in optics the same role as the aspect ratio in hydrodynamics. Therefore we do not consider it a control parameter, and so it remains fixed during each series of experiments. In the same way, but for technical reasons, the experiments presented below have been performed at a constant pump-beam intensity of 10 mW/cm^2. However, we have confirmed that increasing the pump intensity to 20 mW/cm^2 induces only a rescaling of the time by a factor of ~2. Therefore in our experiment the control parameters are (i) the voltage V_0 applied to the crystal, which modifies the gain of the 2WM process, and (ii) the length of the cavity, which acts as a mode selector.

3. DISTRIBUTION OF FAMILIES

Let us first discuss, without consideration of the particular spatial structure or the temporal evolution of the patterns, the influence of the cavity parameters on the families that are able to oscillate. Figures 2 and 3 show phase diagrams of the system as the cavity detuning and V_0 are varied. In these experiments the cavity length is linearly varied over 3λ at the slow rate of $\lambda/300$ s^{-1} while the output pattern of the oscillator is recorded through a video recorder. V_0 is increased stepwise after each sweep is completed. Variations in both directions (increasing and decreasing the cavity length) have been applied to re-

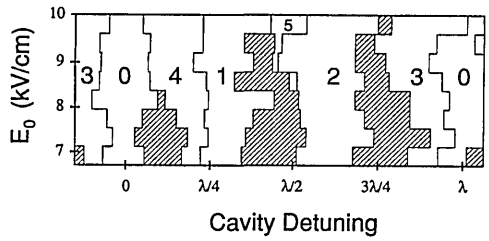

Fig. 2. Phase diagram of a four-mirror PRO as the cavity detuning and the crystal voltage V_0 are varied. The cavity detuning is in length units, and E_0 is the electric field associated with V_0. The regions in which the PRO do not oscillate are hatched. In the other regions a number indicates the family that oscillates.

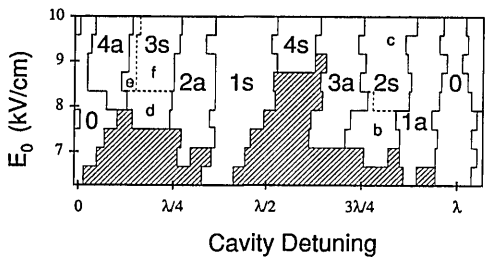

Fig. 3. Same as Fig. 2 for a three-mirror cavity. The notations are the same as in Fig. 2, except that a letter is added to the family number to indicate whether the family is y symmetric (s) or y antisymmetric (a). In the $2s$ family, region b (c) indicates the domain of the H_{02} [$P^{(2)}$] solution. In the $3s$ family region d is associated with the A_{032} pattern, region e with the mode of Fig. 6b (below), and region f with the mode of Fig. 7 (below).

veal any bistabilities. Because each diagram represents acquisitions over a total time of 6 h, thermal shifts of the cavity length were observed. Therefore Figs. 2 and 3 result from the analysis of the video tape but were corrected after we verified that a voltage variation at fixed cavity length has no influence on the oscillating family: we compensated for the main thermal shifts by arbitrarily taking the central frequency of the H_{00} zone as a reference.

Figure 2 is obtained in the case of a 1.35-m-long cavity with four mirrors and $q_c = 5$, which corresponds to a free spectral range of 220 MHz and a transverse intermode spacing of 67 MHz. The numbered areas in Fig. 2 indicate the indices of the family oscillating in each zone, while the hatching denotes nonoscillating regions. The characteristics of the PRO behavior emphasized by this phase diagram may be classified according to the three following points: (i) the PRO response follows the distribution of the empty-cavity modes; i.e., modes with the same frequency have adjacent oscillating domains. This leads to diagrams as simple as Fig. 2, where each family oscillates successively as the cavity length is swept. The oscillating domain of each family is centered on cavity frequencies separated by $\Delta\nu_T = 0.3\Delta\nu_L$, as predicted by the cavity characteristics given at the beginning of this paragraph. The maximum width of the oscillating domain of a family is about $\lambda/4$, corresponding to a frequency width of 55 MHz. The $q = 4$ and the $q = 5$ families fall between lower-q families because $q = 4$ and $q = 5$ families belong to the previous longitudinal mode. (ii) When the crystal dc voltage V_0 is increased, the oscillation starts at a threshold value that increases with the family index q (see also Fig. 3). If V_0 is further increased, the oscillating domain of each family expands. (iii) If V_0 is increased enough so that the oscillating regions of two different families collide, the oscillating domains of each family stops growing, and the two families exclude each other. Bistability between families has not been observed.

Although this behavior seems similar to that observed in lasers, it results from basically different processes, in particular because of the relative values of the gain bandwidth $\Delta\nu$ and of the passive cavity linewidth $\Delta\nu_c$. In lasers, as the cavity length is swept, the emission frequency varies and remains close to the cavity resonance frequency. In contrast, in the PRO a sweep of the cavity length changes only slightly the emission frequency ν, which remains within a few hertz of the maximum gain frequency ν_0. However, as is shown by point (i) of the previous paragraph, the cavity keeps its role of mode selection. In fact the cavity length has a weak influence on the oscillation frequency but fully determines the pattern selected by the PRO. This behavior is close to that of a passive cavity: When the cavity length is tuned, the input field is transmitted when its frequency is close to the cavity frequency, and the width of the transmission curve is determined by $\Delta\nu_c$. In the PRO this width also depends on the gain, and so it decreases for higher-q families, as the intracavity iris introduces larger losses on wider modes, and the width increases with V_0, as observed above. In particular the threshold values of V_0 correspond to the lowest gain values compensating for the losses. However, mutual exclusion of neighboring families at high gain implies strong coupling between these families and is a signature of strong nonlinearities.

To study this last point more precisely, we have built a cavity in which the ratio $\Delta\nu_L/\Delta\nu_T$ is close to an integer, with the aim of reaching a situation in which two different families are in resonance. We observed that in this particular situation modes of the two families contribute to the dynamics according to processes discussed in Section 5 below. At this point we can already conclude that for a given gain and $\Delta\nu_c$ the interaction strength between two adjacent families is determined by the difference between the central resonances of the two families. Unfortunately our experimental setup does not permit the length of the cavity to be varied continuously on an interval large enough to verify this statement accurately.

Figure 3 shows the phase diagram obtained in the case of a 1.8-m-long three-mirror cavity with $q_c = 4$, which corresponds to $\Delta\nu_L = 166$ MHz and $\Delta\nu_T = 66$ MHz. The diagram is changed essentially because of the separation of the y-symmetric and y-antisymmetric modes of each family. Indeed, because of the π inversion phase acquired after one cavity round trip by the y-antisymmetric modes with respect to the y-symmetric modes, the former have a cavity-length resonance shifted by $\lambda/2$ compared with the latter.[17] As a consequence all nonzero q families are split in two new families, referred to as the qs and qa families, where s and a stand for y-symmetric and y-antisymmetric, respectively. If the $q = 0$ family is taken as the origin, the qs families are found to be located in $2.5q\lambda$ modulo λ, as is predicted by the cavity characteristics given above. Note that the $3s$ and $4s$ families appearing in the diagram belong to the longitudinal mode

preceding that of the 0, 1*s*, and 2*s* families. For the *qa* families, shifted from $\lambda/2$ with respect to the *qs* families, three different longitudinal modes appear in Fig. 3, with the 1*a* and 4*a* families reported here being separated by two longitudinal indices. The characteristics of each family are the same as in the four-mirror cavity. In particular, the borders between each family remain well defined, without bistability or coexistence of modes of different families.

The preceding discussion leads to a simple picture of the monofamily behavior of the PRO, which seems quite similar to that of a linear passive cavity. The pattern oscillating for a given cavity length belongs to the closest resonant family and, because of strong frequency pulling, the oscillating frequency ν is always close to that of maximum gain ν_0. The width of the oscillating domain of a family is governed by $\Delta\nu_c$. We also confirmed by measuring $\nu_p - \nu$ through heterodyne detection that the difference $\nu_0 - \nu$ is related, as in any frequency-pulling process, to $\nu - \nu_c$, where ν_c is the empty-cavity mode frequency. The main effect of nonlinearities appears in the mutual exclusion of neighboring families at large gain.

Let us remember that until now we have considered only the global arrangement of the families as a function of the cavity length without taking into account the combinations of modes inside a family. This analysis is done in Section 4 and illuminates intrafamily nonlinear interactions.

4. INTRAFAMILY PATTERNS DISTRIBUTION

The analysis of the patterns oscillating in the PRO has been divided into two steps: the determination of (i) the behavior induced by the simultaneous presence of a small number of different modes in the gain curve of the PRO and (ii) the influence of the loss of preferred directions on this behavior. The two respective stages correspond to the cases of an odd and an even cavity and will be examined successively.

In the three-mirror cavity (Fig. 3) only the modes of same family and same symmetry with respect to the *y* axis interact. This restricts, sometimes drastically, the complexity of the dynamics. For instance, in the $q = 1$ family the only symmetric (antisymmetric) mode is the H_{01} (H_{10}) mode, and in the same way the only antisymmetric mode of the $q = 2$ family is the H_{11} mode. We observed experimentally that in these particular cases the behavior of the oscillator is limited to these stationary patterns (Fig. 4).

The simplest situation in which interaction between several modes can be observed occurs within the symmetric $q = 2$ family. Indeed, the symmetric modes expressed in the usual bases and belonging to this family are the H_{20} and H_{02}, or A_{021} and A_{10}, modes. The observed behavior depends on the parameters of the system as follows. We observed that for a low crystal dc voltage only the H_{02} mode is present (region b in Fig. 3). In contrast, when the voltage is increased (region c in Fig. 3) this stationary pattern disappears in favor of a periodic one that will be referred to below as the $P^{(2)}$ pattern (the exponent is the family index). Snapshots of this pattern regularly distributed over half a period are represented in Fig. 5(a). The $P^{(2)}$ behavior appears as an oscillation between the A_{10} and A_{021} modes. As a function of the time, starting from the A_{10} mode, the pattern slowly evolves to a hybrid mode similar to the 4*H* mode of Ref. 1 and then to the A_{021} mode. During the second half of the period the evolution is reversed. The typical frequency is ~1 Hz. This frequency depends not only on the control parameters but also on the geometry of the cavity.

The time evolution of the intensity of $P^{(2)}$ can be easily reproduced by a simple expression as

$$I_1 \cos^2(\omega t) + I_2 \sin^2(\omega t), \tag{1}$$

where $I_1 = A_1^2$ and $I_2 = A_2^2$ are the intensities of the A_{10} and A_{021} modes, respectively, and $\omega = 2\pi\nu$ is a low frequency. The pattern evolution obtained from this combination [Fig. 5(b)] reproduces well the experimental behavior shown in Fig. 5(a). It is easy to demonstrate that the field amplitude associated with Eq. (1) can be written in the two following equivalent ways:

$$A_1 \cos(\omega t)\cos(\omega' t) + A_2 \sin(\omega t)\sin(\omega' t) \tag{2}$$

or

$$B_1 \cos(\omega_1 t) + B_2 \cos(\omega_2 t), \tag{3}$$

with

$$\omega = \frac{\omega_1 - \omega_2}{2}, \qquad \omega' = \frac{\omega_1 + \omega_2}{2},$$

$$B_1 = \frac{A_1 + A_2}{2}, \qquad B_2 = \frac{A_1 - A_2}{2},$$

where $\omega_1 = 2\pi\nu_1$ and $\omega_2 = 2\pi\nu_2$ are mode angular frequencies. As ω' is an optical frequency, expression (1) is the mean at the ω'^{-1} time scale of the square of expressions (2) or (3). Because of the properties of the Gaussian modes, B_1 and B_2 are here the field amplitudes

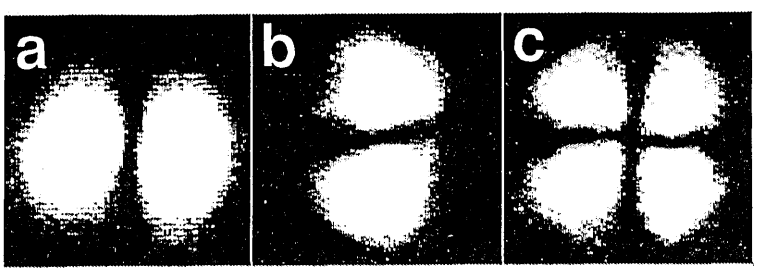

Fig. 4. Stationary modes observed experimentally for the families a, 1*a*; b, 1*s*; and c, 2*a*. As in all following experimental patterns, the zero intensity appears as black while the maximum intensity, i.e., the camera saturation intensity, appears as white.

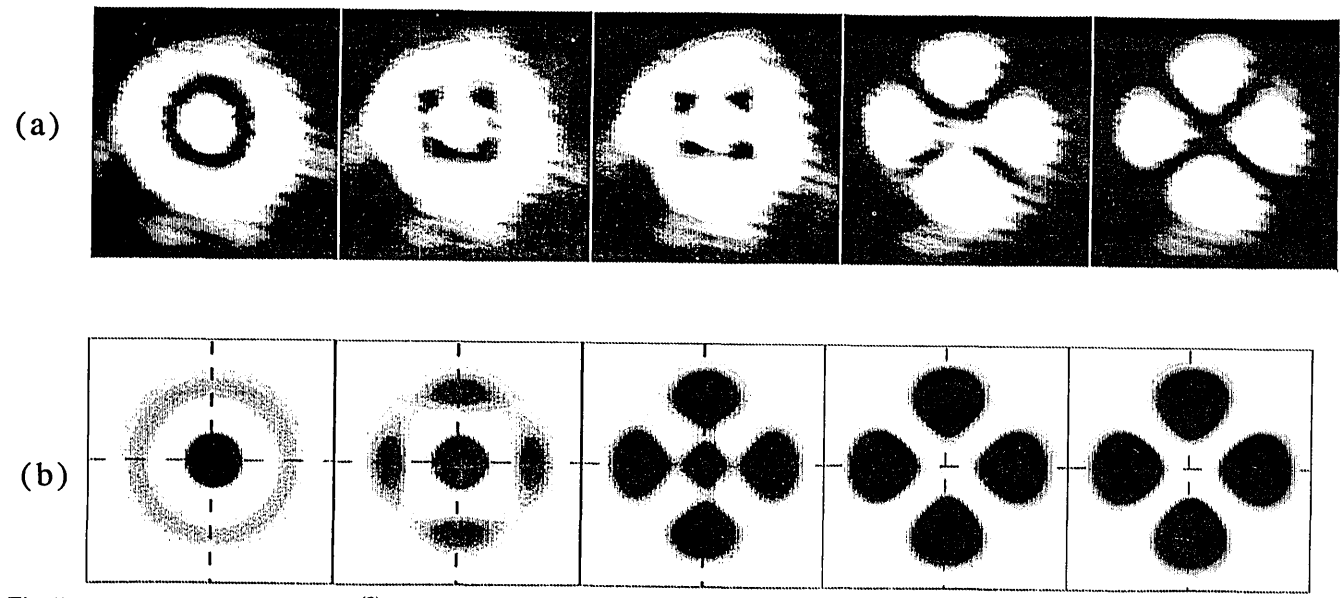

Fig. 5. (a) Half a period of the $P^{(2)}$ pattern observed experimentally in the 2*s* family. The sequence is composed of snapshots of the PRO output at regular intervals for a total duration of ~0.5 s. During the second half of the period the patterns follow the same evolution as in the first half, except reversed in time. (b) Half a period of the pattern obtained by solution of expression (1) for the A_{10} and A_{021} modes. As in all following computed patterns, the intensity has been normalized to its maximum value. Zero intensity appears as white, while the maximum intensity is black. The computed pictures are thus negative images with respect to the experimental ones.

of the H_{02} and H_{20} Hermitian modes. Therefore the $P^{(2)}$ regime appears as the beating between two Hermitian modes. In lasers the same type of behavior has been observed when the astigmatism lifts the degeneracy of two modes of the same family.[3] The behavior observed here could have the same origin. In this case ν_1 and ν_2 are not the original frequencies of the modes but those resulting from the frequency pulling, both within the gain bandwidth, and so separated by $\Delta\nu_a' \cong 1$ Hz. As the oscillating frequency ν depends on the empty-cavity mode frequency ν_c, the value of $\Delta\nu_a'$ is a function of $\Delta\nu_a$. As is mentioned above, this point has been observed experimentally as the sensitivity of the $P^{(2)}$ frequency to the cavity geometry.

The global behavior of the PRO for this family as the control parameters are varied can be understood in the Hermitian basis, for which the two allowed modes are the H_{02} and H_{20} modes. Everything acts as if the H_{20} mode had larger losses than the H_{02} mode. For small V_0 the gain is not large enough, and neither of the two modes oscillates. When V_0 is increased, gain becomes large enough that the H_{02} mode starts to oscillate (region b in Fig. 3). Finally, when V_0 is further increased, the gain becomes so large that even the H_{20} mode, in spite of its larger losses, can oscillate. From this point, because the two modes have different frequencies, a beating between the two modes appears.

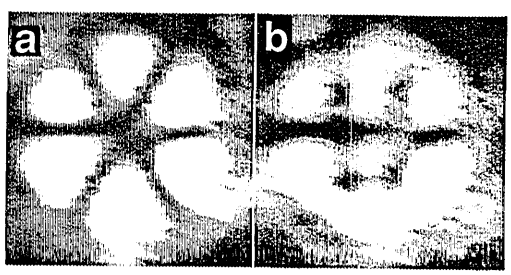

Fig. 6. Stationary modes observed experimentally in the 3*s* family. (a) Mode A_{032} observed in region d of Fig. 3. (b) Hybrid pattern observed in region e of Fig. 3.

This symmetric $q = 2$ family well illustrates the two types of stable patterns that are observed in the weakly multimode PRO: (i) stationary patterns corresponding to the well-known modes of an empty cavity or their linear combinations and (ii) periodic patterns such as the $P^{(2)}$ one. The distribution of the patterns may be more complex than in the $q = 2$ symmetric case, but no other type of behavior has been found. In particular, the dynamical regimes are always periodic and may always be interpreted as the beating of two modes, even when more modes could oscillate in the cavity; quasi-periodic regimes have never been observed for $q_c \leq 5$.

Let us take another example to illuminate this behavior. For the $q = 3$ symmetric family the modes that are theoretically able to oscillate are in the usual bases the H_{03} and H_{21}, or the A_{032} and A_{112}, modes. In Fig. 3 the dashed lines separate regions with different behaviors. In the d and e regions the stationary patterns shown in Fig. 6a (mode A_{032}) and 6b, respectively, are observed. In region f, the regime is an oscillation between the A_{032} and the A_{112} modes (Fig. 7a) with a frequency of ~1 Hz, which is well reproduced by solution of expression (1) for these two modes (Fig. 7b). Note that the global description in terms of Hermite–Gauss modes adopted for the $q = 2$ symmetric family no longer applies here. Indeed, the behavior is now clearly governed by Gauss–Laguerre modes as (i) the stationary pattern associated with smallest losses is the A_{032} mode and (ii) the B_1 and B_2 field patterns appearing in expression (3) are no longer Hermite–Gauss modes. The analysis of behaviors up through the $q = 5$ family shows that the description given by expression (1) with Laguerre–Gauss modes is always relevant. How-

ever, it is expected that, when the Fresnel number is further increased, more complex regimes should be reached.

When one mirror is added to the cavity, the $O(2)$ symmetry of the system is restored, although imperfectly because of several defects such as astigmatism, the planarity of the mirrors, or the birefringence of the optical elements. The first consequence is that the x and the y axes are no longer strongly preferred axes. This lack of orientation induces a complex behavior that can be well illustrated for the $q = 1$ family. Indeed, the basic modes of this family are the H_{10} and H_{01} modes, both constituted by two spots that are opposite in phase. Linear combinations of these modes lead either to the same patterns directed along another direction or to the doughnut modes, depending on their relative phases. The first combination is obtained when privileged directions exist in the system, whereas the second case is obtained in an $O(2)$ symmetry. Thus the observed patterns are good indicators of the effective symmetry of the cavity.

In the PRO the symmetry of the patterns that are effectively observed depends strongly not only on the control parameters but also on the experimental conditions. The doughnut mode, although sometimes observed, is not the dominant regime. In most cases the observed pattern is a two-spot stationary pattern with any direction probably determined by the residual asymmetry of the cavity. In a given experiment this direction is always the same, but a small change in the cavity alignment results in its modification. Because of this high sensitivity of the system to mechanical noise, the stationary regime is often reached after a long periodic transient with a typical frequency of 1 Hz. The time dependence of the pattern may appear as a continuous rotation of the two-spot mode or as an abrupt jump between two differently oriented two-spot modes, with an intermediate doughnut mode. However, the real regime is often a mixing of these two dynamics: The pattern will, e.g., rotate on an angle of 30° and then jump to its initial position. An example of a pattern oscillating between two positions is shown in Fig. 8. The transition between the two directions occurs here through a rotation.

For the other families of modes, the behavior is nearly equivalent: The instantaneous patterns are those already described for an odd cavity, and their time evolution corresponds to a rotation of the main axes of the patterns. The patterns also tend to stabilize after sometimes complicated transients, probably because of the competition between the multimode dynamics and the $O(2)$-symmetry-induced dynamics.

In the preceding results great similarities have been

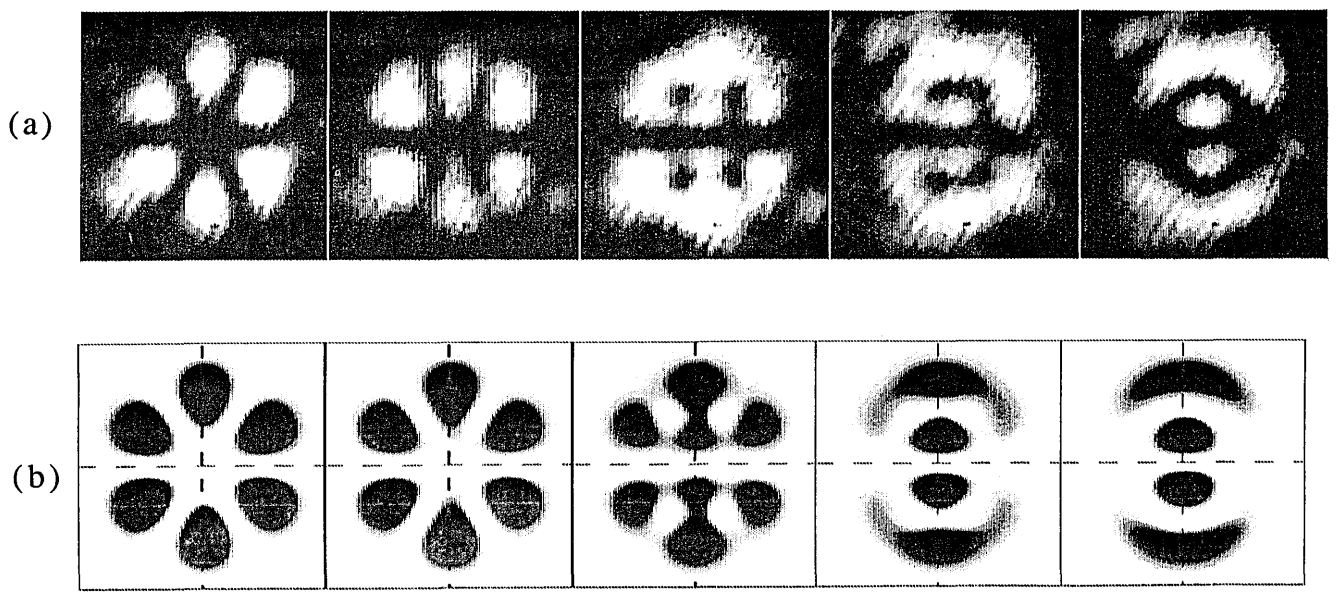

Fig. 7. (a) Half a period of the periodic pattern observed experimentally in the 3*s* family. The sequence is composed of snapshots of the PRO output at regular intervals for a total duration of ~0.5 s. During the second half of its period the patterns follow the same evolution as in the first half, except reversed in time. (b) Half a period of the pattern obtained by solution of Eq. (1) for the A_{11} and A_{032} modes.

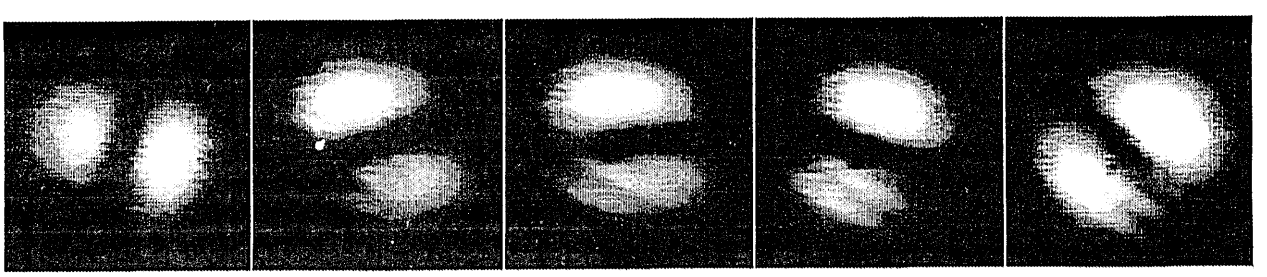

Fig. 8. Example of transient dynamics observed experimentally in a cavity with an even number of mirrors. The sequence is composed of snapshots of the PRO output at regular intervals for a total duration of ~0.5 s. During the second half of its period, the pattern follows the same evolution as in the first half, except reversed in time.

found to the behavior of lasers: the order of appearance of the modes, grouped in families, is the one predicted and observed by Brambilla *et al.*[1]; the dynamical regime obtained when two modes compete, although not predicted by the models, has also been observed experimentally in lasers. However, important differences have to be noted; in particular, bistability between patterns of the same family is never observed, while this behavior is common in lasers.[1]

5. OVERLAPPING OF FAMILIES

This section deals with regimes resulting from the interaction of modes belonging to two different families, while Section 4 was a close look at the mode interaction and patterns behavior inside a given family. This competition may be observed in two different situations: (i) when a control parameter is varied so that the system jumps from one family to another—in this case the competition is only transient—and (ii) in the particular situation in which two different families have resonance frequencies close enough to each other so that both oscillate simultaneously, as shown in Section 3. Because in the second case the competition is permanent, let us, for the sake of clarity, examine such a configuration first.

A three-mirror cavity with $\Delta\nu_L/\Delta\nu_T \cong 8$ is built, so that the $q = 0$ and $4a$ families are in quasi-resonance. A periodic pattern is obtained with a cavity length for which the two families interact. Half a period of the pattern is shown in Fig. 9(a). The evolution appears as an oscillation with a period of ~1 Hz between two cross-shaped patterns that are shifted with respect to each other by an angle of $\pi/4$. During this time the pattern never has the shape of a Hermite–Gauss or a Laguerre–Gauss mode.

To understand the mechanisms leading to such behavior, we tried, as in Section 4, to model it with a simple equation. When expression (1) is used, the patterns associated with I_1 and I_2 are the two crossed patterns described above. However, a description using the Laguerre–Gauss modes seems more appropriate here, as these modes are those oscillating when no interaction between families occurs. In this case the intensity evolution of the pattern has to be described by an expression of the following type:

$$[A_1 \cos(\omega t) + A_2 \sin(\omega t)]^2, \tag{4}$$

where A_1 and A_2 are the field amplitudes of the A_{00} and A_{042} modes, respectively. Figure 9(b) shows half a period of the pattern obtained from this equation. To explain the difference between this behavior and expression (1), let us write the field amplitude associated with expression (4), including the optical frequency. In the same way as for expression (2), we obtain

$$A_1 \cos(\omega t)\cos(\omega' t) + A_2 \sin(\omega t)\cos(\omega' t), \tag{5}$$

with the same notation as in expression (2). The only difference between expressions (2) and (5) is the relative phase of the fast term of the two modes A_1 and A_2. In expression (5) the A_1 mode varies as $\cos(\omega' t)$, whereas in expression (2) it varies as $\sin(\omega' t)$, and so the two modes evolve in quadrature on both the slow and the fast time scales. The result is that, globally, the two modes interact in phase and in opposite phase, as shown in expression (3) by the terms $A_1 \pm A_2$. In contrast, in expression (5) the two modes vary as $\cos(\omega' t)$, and so add to each other globally in quadrature because of the slow term. From another point of view, the modes interact here with an interference term, whereas inside a family they alternate without interfering.

The origin of the slow frequency is here again to be found in the spectrum narrowing induced by the strong frequency pulling on the oscillating frequencies. Indeed, because of the imperfection of the alignment, it can be

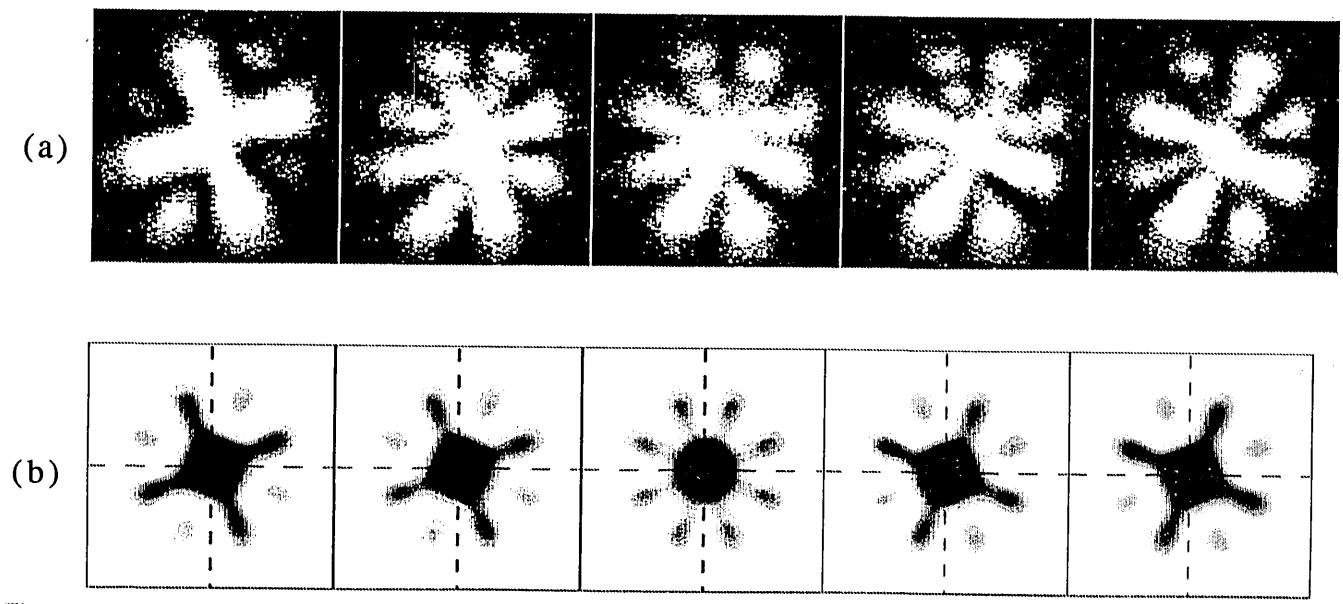

Fig. 9. (a) Half a period of the periodic pattern observed experimentally when the $q = 0$ and $4a$ families are degenerate. The sequence is composed of snapshots of the PRO output at regular intervals for a total duration of ~0.5 s. During the second half of its period, the pattern follows the same evolution as in the first half, except reversed in time. (b) Half a period of the pattern obtained by computation of expression (4) for the A_{00} and A_{042} modes.

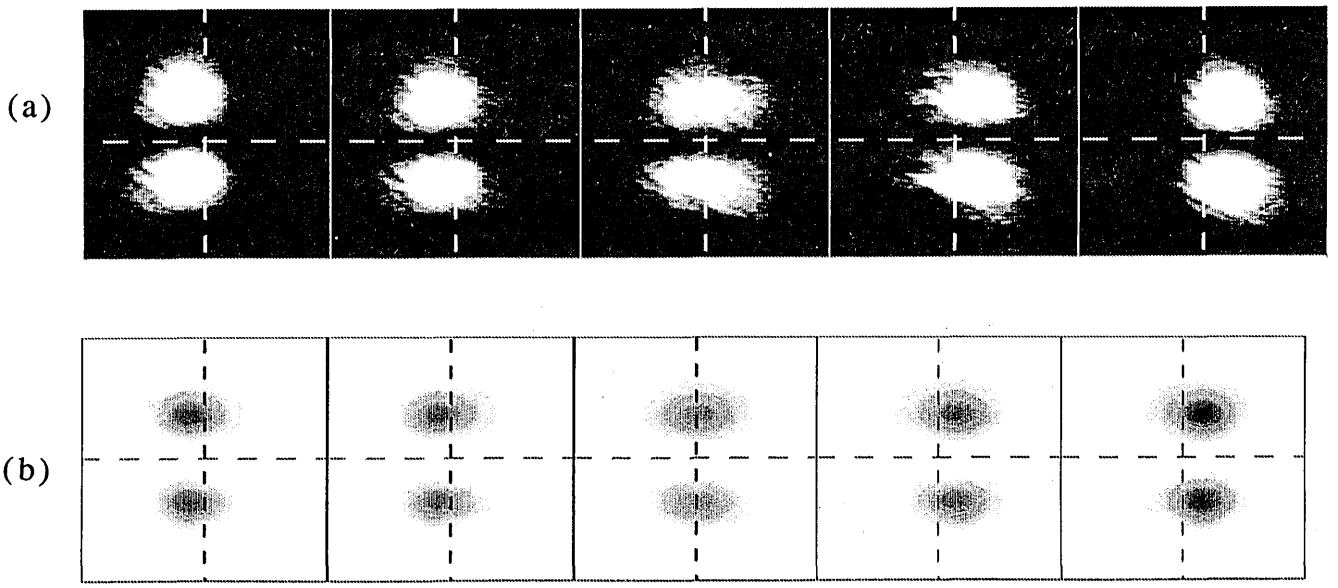

Fig. 10. (a) Half a period of the periodic transient observed experimentally after a change in the cavity length from the H_{01} mode to the H_{11} mode. The sequence is composed of snapshots of the PRO output at regular intervals for a total duration of ~0.2 s. The transverse character of the regime consists of a time variation of the amplitude between the extreme positions of the two spots from zero to a value equal to the distance between the two spots. (b) Half a period of the pattern obtained by computation of expression (4) for the H_{01} and H_{11} modes.

supposed that the resonance frequencies of the two families are separated by at least some kilohertz. This difference is reduced to a frequency in the range of 1 Hz because of the frequency pulling, by the same mechanism as that described in Section 3 for the astigmatism-induced frequency split.

This behavior is not specific to the mixing of the $q = 0$ and $4a$ families and has been observed whatever the two interacting families. Moreover, the same type of interaction is observed during the transient behavior resulting from the jump from one family to another. Figure 10(a) illustrates the transition from $1s$ to $2a$ families as obtained in the phase diagram of Fig. 3 for $E_0 = 10$ kV/cm when the cavity length is increased adiabatically from 0.37λ. When the border between the two families is crossed, the H_{01} mode, which is no longer stable, is transformed into the H_{11} mode through a periodic transient. The two spots of the H_{01} mode start to move back and forth with a transverse amplitude between extreme positions, which increases as a function of time, until the H_{11} mode is reached.

This behavior results from a combination similar to that observed in the degenerate case. Therefore expression (4) may be used to reproduce the experimental behavior if a damped term is added to take into account the transient character of the regime. The behavior described by expression (4) with the H_{01} and H_{11} modes [Fig. 10(b)] reproduces the experimental observations well. The crossing of any border separating the families in the parameter space leads to the same type of behavior.

In terms of nonlinear dynamics, the stable periodic pattern obtained in the degenerate case may be interpreted as the competition of two stable modes. Therefore the transient behavior observed here could originate from the coexistence of one stable mode and one unstable mode. This hypothesis is confirmed by the following experiment: When the cavity length is swept at a frequency of ~10 Hz around a transition between two families, the stable solutions are extended in their unstable region, and the observed bistability cycle has the shape of a butterfly. Therefore it appears that when two modes of two different families have resonance frequencies that differ enough, a strong coupling between them results in a winner-take-all dynamics: The transition in the parameter space from one mode to the other one is abrupt, without coexistence or bistability. On the other hand, if the two modes have close enough resonance frequencies, the interaction results in a dynamical regime.

Thus it appears that the way two modes with different frequencies interact depends strongly on whether they belong to the same family or not. This means that the oscillator is able to recognize two modes of the same family even if they do not have the same frequency. Thus this classification in families, originally done as a function of the frequencies, here takes another meaning, probably linked to the geometry of the modes.

6. CONCLUSION

This study deals with stationary and periodic regimes observed in a weakly multimode PRO. We show that in this system the modes of the empty cavity and their families are relevant for the analysis of transverse patterns, as in a laser. The global behavior of the PRO is also close to that observed in lasers, in spite of fundamentally different physical mechanisms. The observed divergences from laserlike behavior reveal the definitive characteristics of the PRO as large frequency pulling or strong mode coupling. The main consequences are the very small characteristic times (~1 s) of the dynamics and the absence of multistability between patterns. Different types of dynamics have been observed from different origins:

optical nonlinearities, $O(2)$ symmetry, and astigmatism. On the basis of the knowledge of the PRO dynamics in the multimode configuration, it is now possible to investigate other ranges of parameters, in particular those leading to highly multimode operation.

ACKNOWLEDGMENTS

We thank J.-P. Huignard, H. Rajbenbach, and A. Delboulbé of the Laboratoire Central de Recherche of Thomson (Orsay, France) for technical help and useful discussions as well as for the loan of photorefractive crystals. This research was supported by Direction des Recherches, Etudes et Techniques contract 92101.

REFERENCES

1. M. Brambilla, F. Battipede, L. A. Lugiato, V. Penna, F. Prati, C. Tamm, and C. O. Weiss, "Transverse laser patterns," Phys. Rev. A **43,** 5090–5120 (1991).
2. M. Brambilla, M. Cattaneo, L. A. Lugiato, R. Pirovano, F. Prati, A. J. Kent, G. L. Oppo, A. B. Coates, C. O. Weiss, C. Green, E. J. D'Angelo, and J. R. Tredicce, "Dynamical transverse laser patterns," Phys. Rev. A (to be published).
3. D. Hennequin, C. Lepers, E. Louvergneaux, D. Dangoisse, and P. Glorieux, "Spatio-temporal dynamics of a weakly multimode CO_2 laser," Opt. Commun. **93,** 318–322 (1992).
4. D. Dangoisse, D. Hennequin, C. Lepers, E. Louvergneaux, and P. Glorieux, "2D optical lattices in a CO_2 laser," Phys. Rev. A **46,** 5955–5958 (1992).
5. P. Coullet, L. Gil, and F. Rocca, "Optical vortices," Opt. Commun. **73,** 403–408 (1989).
6. A. C. Newel and J. V. Moloney, *Nonlinear Optics* (Addison-Wesley, Redwood City, Calif., 1992).
7. C. O. Weiss, H. R. Telle, K. Staliunas, and M. Brambilla, "Restless optical vortex," Phys. Rev. A **47,** R1616–R1619 (1993).
8. R. Graham and H. Haken, "Laserlight—first example of a second-order phase transition far away from thermal equilibrium," Z. Phys. **237,** 31–46 (1970).
9. F. T. Arecchi, G. Giacomelli, P. L. Ramazza, and S. Residori, "Vortices and defect statistics in two-dimensional optical chaos," Phys. Rev. Lett. **67,** 3749–3752 (1991).
10. S. A. Akhmanov, M. A. Vorontsov, V. Y. Ivanov, A. V. Larichev, and N. I. Zheleznykh, "Controlling transverse-wave interactions in nonlinear optics: generation and interaction of spatiotemporal structures," J. Opt. Soc. Am. B **9,** 78–90 (1992).
11. R. Macdonald and H. J. Eichler, "Spontaneous optical pattern formation in a nematic liquid crystal with feedback mirror," Opt. Commun. **89,** 289–295 (1992).
12. H. Rajbenbach and J.-P. Huignard, "Self-induced coherent oscillations with photorefractive $Bi_{12}SiO_{20}$ amplifier," Opt. Lett. **10,** 137–139 (1985).
13. F. T. Arecchi, G. Giacomelli, P. L. Ramazza, and S. Residori, "Experimental evidence of chaotic itinerancy and spatio-temporal chaos in optics," Phys. Rev. Lett. **65,** 2531–2534 (1990).
14. R. Blumrich, T. Kobialka, and T. Tschudi, "Behavior of the self-oscillation pattern in a phase-conjugate ring resonator," J. Opt. Soc. Am. B **7,** 2299–2305 (1990); S. R. Liu and G. Indebetouw, "Periodic and chaotic spatiotemporal states in a phase-conjugate resonator using a photorefractive $BaTiO_3$ phase-conjugate mirror," J. Opt. Soc. Am. B **9,** 1507–1520 (1992).
15. G. C. Valley and G. J. Dunning, "Observation of optical chaos in a phase-conjugate resonator," Opt. Lett. **9,** 513–515 (1984).
16. L. Dambly and H. Zeghlache, "Frequency shift in an oscillator with photorefractive gain," Phys. Rev. A **47,** 2264–2275 (1993).
17. S. A. Collins and D. T. M. Davis, "Modes in a triangular ring optical resonator," Appl. Opt. **3,** 1314–1315 (1964).